Monthly Notices
of the
ROYAL ASTRONOMICAL SOCIETY

MNRAS **432,** 810–821 (2013)
Advance Access publication 2013 April 19

doi:10.1093/mnras/stt491

Implications of the kinematical structure of circumnuclear star-forming regions on their derived properties

Guillermo F. Hägele,[1,2,3]★ Ángeles I. Díaz,[3] Roberto Terlevich,[4,5] Elena Terlevich,[4]†
Guillermo L. Bosch[2] and Mónica V. Cardaci[1,2,3]

[1]*IALP-Conicet, Paseo del Bosque s/n, 1900 La Plata, Argentina*
[2]*Facultad de Ciencias Astronómicas y Geofísicas, Universidad Nacional de La Plata, Paseo del Bosque s/n, 1900 La Plata, Argentina*
[3]*Departamento de Física Teórica, C-XI, Universidad Autónoma de Madrid, 28049 Madrid, Spain*
[4]*Instituto Nacional de Astrofísica Óptica y Electrónica, L.E. Erro No. 1, Santa María Tonantzintla, Puebla, México*
[5]*Institute of Astronomy, University of Cambridge, Madingley Road, Cambridge CB3 0HA, UK*

Accepted 2013 March 18. Received 2013 March 12; in original form 2012 November 9

ABSTRACT

We review the results of high-dispersion spectroscopy of 17 circumnuclear star-forming regions (CNSFRs) in 3 nearby early spiral galaxies, NGC 2903, NGC 3310 and NGC 3351. We find that single-Gaussian fitting to the Hβ and [O III]λ5007 Å line profiles results in velocity dispersions around 32 and 52 km s^{-1}, respectively, while the IR Ca II triplet cross-correlation technique provides stellar velocity dispersion values close to 50 km s^{-1}. Even though multiple kinematical components are present, the relation between gas velocity dispersion and Balmer emission line luminosity (L–σ relation) reproduces the correlation for disc giant H II regions albeit with a larger scatter. The scatter in the L–σ relation is considerably reduced when theoretical evolutionary corrections are applied suggesting that an age range is present in the sample of CNSFRs. To analyse the observed complex profiles, we performed multiple Gaussian component fits to the Hβ and [O III]λ5007 Å lines obtaining optimal fits with two Gaussians of different widths. These best fits indicate that the narrower component has average velocity dispersion close to 23 km s^{-1} while the broader component shows average values in the range 50–60 km s^{-1} for both lines, close to the observed stellar velocity dispersions. The fluxes of the broad and narrow Hβ components are similar. This is not the case for [O III]λ5007 Å for which the broad components have higher fluxes than the narrow ones, thus producing a clear segregation in their [O III]/Hβ ratios. We suggest a possible scenario for understanding the behaviour of CNSFRs in the L–σ and $\sigma_{\rm gas}$–σ_* diagrams involving an inner gaseous disc responsible for the narrow component of the emission lines. Our main conclusion is that the presence of different kinematical components with similar total fluxes in the emission line spectrum of CNSFRs raises important doubts regarding the properties of the ionized gas derived from global line ratios obtained with low-resolution spectroscopy in star-forming regions in the central regions of early-type galaxies. Given the ubiquity of these star-forming systems, ionized gas analyses should be done preferably from high-dispersion spectra with high spatial resolution.

Key words: H II regions – galaxies: kinematics and dynamics – galaxies: starburst – galaxies: star clusters: general.

1 INTRODUCTION

Star formation in a circumnuclear configuration is of common occurrence in early spiral galaxies with or without an active nucleus. These structures are frequently arranged in a ring pattern with a diameter of about 1 kpc (Morgan 1958; Sérsic & Pastoriza 1965,

★ E-mail: ghagele@fcaglp.unlp.edu.ar
† Visiting astronomer at IoA, University of Cambridge, UK.

1967) and their associated star formation rate (SFR) is considerably higher than the average observed in galactic discs. In fact, in the ultraviolet (UV), the luminosity coming from their young massive stars can dominate the observed circumnuclear emission even in the presence of an active nucleus (González-Delgado et al. 1998; Colina et al. 2002).

The properties of circumnuclear star-forming regions (CNSFRs) are different enough from giant extragalactic H II regions that they can be considered to constitute a distinctive mode of star formation in galaxies (Kennicutt 1998). This distinct nature was fully revealed with the opening of the mid- and far-IR spectral ranges (see for example Rieke & Low 1972; Harper & Low 1973; Rieke & Lebofsky 1978; Telesco & Harper 1980). CNSFRs look more compact and show higher peak surface brightness than disc H II regions (Kennicutt, Keel & Blaha 1989) while their optical spectra show the weak oxygen forbidden lines characteristic of a high abundance (Díaz et al. 2007, hereafter D07).

It has been suggested that the substructures (sizes of the order of 10 pc or less) found in circumnuclear star-forming complexes correspond to massive ($M \sim 10^5$ M$_\odot$) young (age $\lesssim 1$ Gyr) clusters. If this is the case, they can be modelled as single stellar population applying population synthesis techniques, and their properties such as age, chemical evolution and star formation histories could be derived with only small uncertainties due to discreteness-related scatter (see e.g. Cerviño et al. 2002). Although there have been some recent works devoted to the study of CNSFRs, most of them have concentrated in deriving the SFR and ages of these structures and little has been done with respect to their structure and internal kinematics.

In the last few years, we have obtained spectroscopic data of CNSFRs in nearby galaxies with a resolution enough to allow the measurement of stellar and gaseous velocity dispersions that, combined with their sizes obtained from the *Hubble Space Telescope* (*HST*) imaging, have yielded values for the dynamical masses of these objects (Hägele et al. 2007, 2009, 2010a, hereafter H07, H09 and H10, respectively). In this paper, we present the results obtained from the joint analysis of the data and address several aspects related to the properties of these structures. In particular, we analyse the relations between stellar and gaseous velocity dispersions and the behaviour of the velocity dispersion–luminosity (σ–L) and mass–luminosity (M–L) relations for CNSFRs. We also draw attention to several concerns related to conclusions about gas properties of central regions of galaxies, like average chemical abundances or characteristics of ionizing sources, derived from data with low spatial and spectral resolution.

2 SUMMARY OF DATA AND DERIVED PARAMETERS

The CNSFRs studied in this work correspond to three early-type barred spiral galaxies, NGC 2903, NGC 3310 and NGC 3351, whose properties are given in Table 1.

For 17 star-forming complexes, we obtained high-resolution spectroscopy in the blue (4779 to 5199 Å) and red (8363 to 8763 Å) with resolutions of 0.21 and 0.39 Å pixel^{-1}, respectively, providing a comparable velocity resolution of about 13 km s^{-1}. The blue spectral region comprises the emission lines of Hβ λ4861 Å and [O III] λ5007 Å and have been used to measure the gas velocity dispersion. The red spectral region comprises the stellar absorption lines of the Ca II triplet (CaT) at $\lambda\lambda$8494, 8542, 8662 Å, and have been used to measure the stellar velocity dispersion. The two spectra have been obtained simultaneously using the double-arm Intermediate-dispersion Spectrograph and Imaging System attached to the William Herschel Telescope, and therefore we are confident that they refer to the same regions. More details about the observations can be found in our previous works (H07; H09; H10).

Table 1. The galaxy sample.

Property	NGC 2903	NGC 3310	NGC 3351
RA (2000)[a]	09 32 10.1	10 38 45.9	10 43 57.7
Dec. (2000)[a]	+21 30 03	+53 30 12	+11 42 14
Morph. type	SBbc	SABbc	SBb
Distance (Mpc)	8.6 ± 0.5[b]	15 ± 1[a]	10.05 ± 0.88[c]
pc/arcsec	42 ± 2	73 ± 5	49 ± 4
B_T (mag)[a]	9.7 ± 0.1	11.2 ± 0.1	10.5 ± 0.1
$E(B-V)_{\rm gal}$(mag)[a]	0.031 ± 0.01	0.030 ± 0.01	0.028 ± 0.01

[a]de Vaucouleurs et al. (1991).
[b]Bottinelli et al. (1984).
[c]Graham et al. (1997).

The velocity dispersions of the gas, $\sigma_{\rm gas}$, were calculated as

$$\sigma_{\rm gas} = \sqrt{\sigma_{\rm m}^2 - \sigma_{\rm i}^2}, \quad (1)$$

where $\sigma_{\rm m}$ and $\sigma_{\rm i}$ are the measured and instrumental dispersions, respectively, in km s^{-1}. $\sigma_{\rm i}$ was measured directly from the sky emission lines and is about 10.4 km s^{-1} at λ4861 Å. No thermal broadening correction was applied; thus, our dispersions slightly overestimate the gas intrinsic dispersion.

The single-component Gaussian fits performed to the Hβ line were not totally satisfactory. In fact, in all cases, the optimal fit was found for two different Gaussian components. In most cases, similar components also provided optimal fits to the [O III] lines. Fig. 1 shows fits to the Hβ lines in CNSFRs of each of the three galaxies studied as illustrative examples.

The stellar velocity dispersions, σ_*, were estimated from the CaT lines by cross-correlating the spectrum corresponding to each of the regions with stellar templates. An example of the CaT spectral region can be seen in Fig. 2.

When observed with the *HST* resolution, most of the observed CNSFRs seem to be a composite of more than one cluster with radii between 1.5 and 6.2 pc. The virial theorem has been applied to estimate upper limits to the dynamical masses inside the half-light radius for each identified knot under the assumption that the clusters are gravitationally bound, spherically symmetric and have isotropic velocity distributions [σ^2(total) = $3\sigma_*^2$]. The general expression for the virial mass of a cluster is

$$M_* = \eta\, \sigma_*^2\, R/G, \quad (2)$$

where R is the effective gravitational radius and η is a dimensionless number that takes into account departures from isotropy in the velocity distribution and the spatial mass distribution, binary fraction, mean surface density, etc. (Boily et al. 2005; Fleck et al. 2006). Following Ho & Filippenko (1996a,b), and for consistence with H07, H09, H10 and Hägele (2008), we obtain the dynamical masses inside the half-light radius using $\eta = 3$ and adopting the half-light radius as a reasonable approximation of the effective radius. Since our measured stellar velocity dispersion encompasses each whole region to which the single clusters belong, their masses can be overestimated to some extent. However, we think that the mass overestimate cannot be large, because the equivalent widths of the CaT lines point to the spectral energy distribution of each region being dominated by the young stellar population belonging to the clusters rather than by the galaxy bulge. The adopted mass

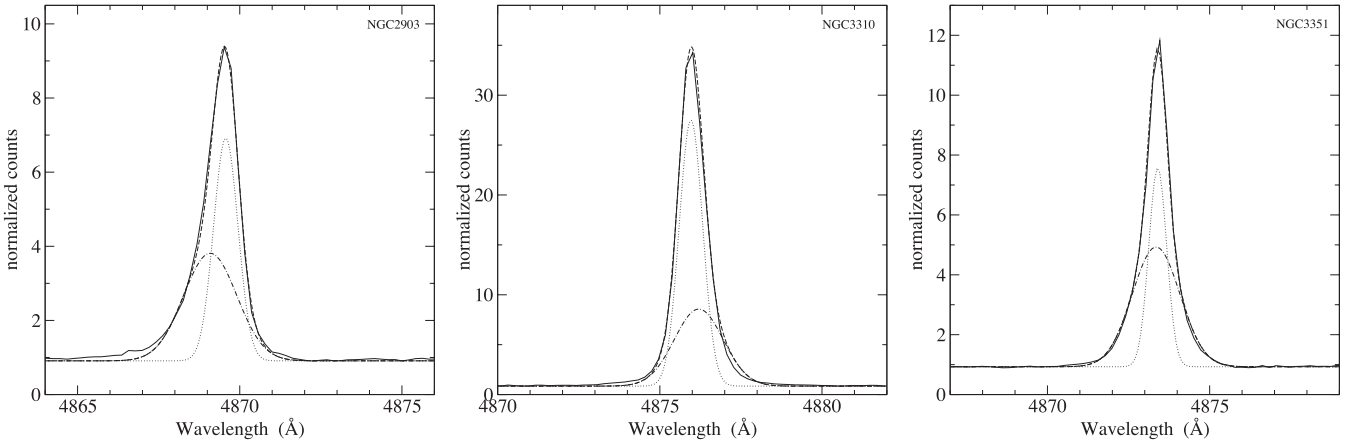

Figure 1. Optimal Gaussian fits to the Hβ line for observed regions in the galaxies: NGC 2903, NGC 3351 and NGC 3310. The two different components labelled 'broad' and 'narrow' are shown.

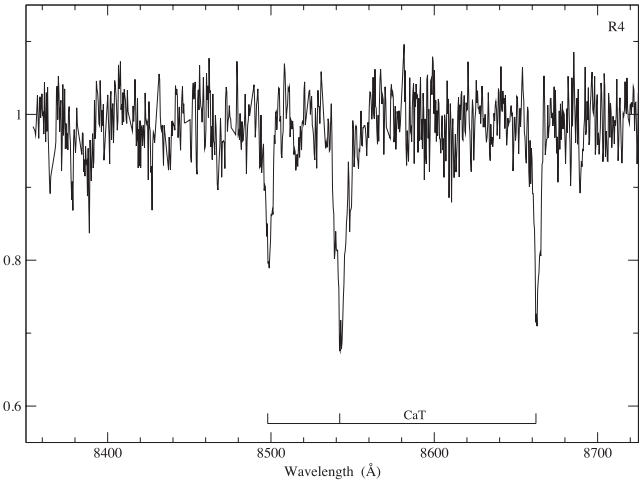

Figure 2. Spectrum of region R4 in NGC 2903 in the IR CaT spectral region.

for each region has been obtained by summing up the individual masses of the single clusters. More details about these procedures can be found in H07.

Table 2 lists the velocity dispersions in each CNSFR together with the derived values of the dynamical masses. Column 1 gives the name of the region as coded in the original publication; column 2 gives the stellar velocity dispersion (σ_*); column 3 gives the value of the gas velocity dispersion derived using a single-Gaussian fit (σ_s) to the Hβ line; columns 4 and 5 give the corresponding values derived by the two-component optimal fit that have been labelled narrow (σ_n) and broad (σ_b), respectively. Columns 6 to 8 provide the same information for the [O III] emission lines. Finally, column 9 gives the derived dynamical mass, M_{ast}.

There are three objects with two sets of values listed in the table which correspond to different observations acquired in two different slit position angles.

For every region we have derived the mass of the ionizing stellar population, (M_{ion}), from published values of the Hα luminosity (Pastoriza et al. 1993; Planesas, Colina & Pérez-Olea 1997; Díaz et al. 2000a) corrected for reddening assuming the galactic extinction law of Miller & Mathews (1972) with $R_V = 3.2$ and, when necessary, correcting for recent changes in their distances. The solar metallicity [12 + log(O/H) = 8.919] single-burst models by García-Vargas, Bressan & Díaz (1995) were used. These models assume a Salpeter initial mass function (Salpeter 1955) with lower and upper mass limits of 0.8 and 120 $M_\odot$ and provide the number of ionizing Lyman continuum photons [$Q(H_0)$] per unit mass of the ionizing population, [$Q(H_0)/M_{ion}$]. This number decreases with the time evolution of the population, and is related to the computed equivalent width (EW) of the Hβ line as (e.g. Díaz et al. 2000b)

$$\log\left[Q(H_0)/M_{\rm ion}\right] = 44.48 + 0.86\log\left[\mathrm{EW(H}\beta)\right]. \quad (3)$$

The total number of ionizing photons for a given region has been derived from the Hα luminosities (Leitherer & Heckman 1995):

$$Q(H_0) = 7.35 \times 10^{11}\, L(\mathrm{H}\alpha). \quad (4)$$

The final expression for the derivation of M_{ion} is then

$$M_{\rm ion} = \frac{7.35 \times 10^{11}\, L(\mathrm{H}\alpha)}{10^{44.48\,+\,0.86\,\log[\mathrm{EW(H}\beta)]}}. \quad (5)$$

The EWs of the Hβ line have been taken from Pastoriza et al. (1993) and D07. Given that the Hβ EWs are probably affected by an underlying older stellar continuum not belonging to the ionizing cluster itself, the listed masses for these clusters should be considered upper limits. On the other hand, no photon escape or absorption of ionizing photons by dust has been considered, which would place lower limits to the mass. These two effects probably cancel each other to a certain degree.

The mass of ionized gas ($M_{\rm H\,II}$) associated with each star-forming region complex was derived from the Hα luminosities, using the electron density (N_e) dependence relation given by Macchetto et al. (1990) for an electron temperature of 10^4 K,

$$M_{\rm H\,II} = 3.32 \times 10^{-33}\, L(\mathrm{H}\alpha)\, N_e^{-1}. \quad (6)$$

The electron density for each region was taken from Pastoriza et al. (1993) and D07. For those regions of NGC 3310 without electron density estimates, a value of N_e equal to 100 cm^{-3}, corresponding to the average value of other CNSFRs of this galaxy, was assumed.

The values of the Hα luminosities for each CNSFR together with quantities derived from them are given in Table 3. Also in this table, and following the work by Relaño & Beckman (2005), we list the individual Gaussian component fluxes as fractional emission (EM*f*), in percentage, relative to the total line flux.

These have been calculated from the emission line fluxes estimated for each Hβ component from the parameters derived using

Table 2. Velocity dispersions and dynamical masses for the observed CNSFR.

Region	σ_*	Hβ σ_s	Hβ σ_n	Hβ σ_b	[O III] σ_s	[O III] σ_n	[O III] σ_b	M_*
				NGC 2903				
R1+R2	60±3	34±2	23±2	51±3	73 ± 8	26 ± 8	93 ± 9	1816±48
R1+R2	64±3	35±2	27±2	53±4	71 ± 9	27 ± 7	95 ± 10	2054±45
R4	44±3	32±2	20±2	47±4	76 ± 10	35 ± 9	89 ± 8	853±28
R7	37±3	32±4	29±5	34±8	59 ± 10	17 ± 5	67 ± 8	642±26
				NGC 3310				
R1+R2	80:	33±4	24±5	54±7	31 ± 4	22 ± 5	50 ± 4	911:
R4	36±3	34±3	28±4	55±5	32 ± 3	26 ± 3	52 ± 4	886 ±30
R4+R5	38±3	27±4	22±4	46±5	22 ± 3	18 ± 3	40 ± 2	1317 ±41
R6	35±5	30±3	23±3	54±7	28 ± 3	21 ± 3	56 ± 3	397 ±33
S6	31±4	27±3	20±3	47±4	26 ± 3	19 ± 3	47 ± 3	210 ±17
R7	44±5	21±5	18±4	41±4	17 ± 4	14 ± 3	36 ± 3	1413±60
R10	39±3	38±3	26±2	54±2	40 ± 3	26 ± 3	59 ± 4	588 ±28
J	–	34±2	25±2	61±3	30 ± 2	22 ± 2	57 ± 3	–
				NGC 3351				
R2	50±1	26±1	17±3	45±3	72 ± 7	21 ± 4	74 ± 5	129±6
R2	51±6	29±3	16±2	43±2	69 ± 9	23 ± 5	76 ± 8	131±23
R3	55±5	35±1	25±3	59±4	67 ± 7	28 ± 4	71 ± 4	417±31
R3	59±7	39±5	24±3	59±3	70 ± 7	24 ± 6	74 ± 9	477±47
R4	66±4	37±4	29±3	65±4	76 ± 8	–	–	87±12
R5	47±4	34±2	30:	76:	56 ± 7	–	–	49±8
R6	39±6	29±6	16±3	46±4	46 ± 7	–	–	434±39

Note: velocity dispersions in km s^{-1}, masses in 10^5 M$_\odot$. The colons instead of the corresponding errors indicate that those quantities have large associated errors (greater than 40 per cent).

Table 3. Hα luminosities and derived quantities, and Hβ EWs.

Region	$L(\mathrm{H}\alpha)_t$	EMf_n	EMf_b	$L(\mathrm{H}\alpha)_n$	$L(\mathrm{H}\alpha)_b$	M_{ion}	M_{HII}	EW(Hβ)
				NGC 2903				
R1+R2	66.3[a]	49	51	32.3	34.0	18.9	0.79	12.1
R1+R2	–	57	43	38.1	28.2	–	–	12.1
R4	38.9[a]	32	68	12.6	26.3	24.6	0.48	4.8
R7	31.3[a]	59	41	18.6	12.7	23.6	0.30	3.9
				NGC 3310				
R1+R2	102[b]	48	52	49.3	52.7	13.9	3.38	28.6
R4	144[b]	58	42	83.5	60.5	17.6	4.78	32.4
R4+R5	218[b]	62	38	136	82.0	21.4	7.24	41.7
R6	57.3[b]	53	47	30.5	26.8	12.4	1.90	16.7
S6	62.5[c]	54	46	34.0	28.5	17.4	2.07	12.5
R7	45.5[b]	72	28	32.7	12.8	8.7	1.51	19.4
R10	45.5[b]	39	61	18.0	27.5	15.7	1.51	9.7
J	573[b]	51	49	294	279	31.4	9.52	82.5
				NGC 3351				
R2	28.3[a]	40	60	11.4	16.9	9.93	0.21	9.5
R2	–	35	65	10.0	18.3	–	–	9.5
R3	70.0[a]	49	51	34.4	35.7	15.3	0.54	16.5
R3	–	33	67	22.9	47.1	–	–	16.5
R4	23.2[a]	48	52	11.1	12.1	6.23	0.25	13.0
R5	10.3[a]	80	20	8.2	2.1	6.17	0.09	5.1
R6	7.5[a]	46	54	3.4	4.0	8.88	0.07	2.3

Note: EMf in percentage, luminosities in 10^{38} erg s^{-1}, masses in 10^5 M$_\odot$.
[a]From Planesas et al. (1997) corrected for the different adopted distances, and for reddening using $E(B-V)$ from Pérez-Olea (1996).
[b]From Díaz et al. (2000a).
[c]From Pastoriza et al. (1993).

the fitting from the NGAUSS task of IRAF.[1] Individual component Hα luminosities follow directly from those with the only assumptions that the reddening corrections are the same for both components (although this is not necessarily true, see Hägele et al. 2012) and that the EM*f* remains constant across the whole nebula. It must be noticed that the slit is 1 arcsec wide, and the estimated diameters of the entire star-forming complexes from which the photometric fluxes were estimated are about 2 arcsec.

As in the case of Table 2 there are several objects with two sets of values listed in Table 3 which correspond to two different observations as explained above.

3 DISCUSSION

3.1 Star and gas kinematics

Given the emission line profile differences between permitted and forbidden lines already reported by us in previous works (H07; H09; H10), it is important to study the relationship between the velocity dispersion of the stars and the ionized gas for all the CNSFRs that have been observed at high dispersion and with similar instrumentation.

A quick inspection of Table 2 shows that while the stellar velocity dispersion in the CNSFRs ranges between ∼30 and ∼75 km s^{-1} with an average value of 49 km s^{-1}, the ionized gas velocity dispersion, as obtained from the Hβ emission line using a single-Gaussian fit, shows a range between ∼20 and ∼40 km s^{-1} with an average value of 32 km s^{-1}. On the other hand, the [O III] velocity dispersion, also measured from a single-Gaussian fit, that ranges between ∼17 and ∼75 km s^{-1} with an average value of 52 km s^{-1} has values closer to the stellar velocity dispersion perhaps indicating some extra source of broadening with respect to Hβ (see a detailed discussion in H09).

The systematic shift between the ionized gas and stellar velocity dispersion is clearly seen in Fig. 3 that shows the gas velocity dispersion measured by fitting a single Gaussian to the Hβ and [O III] lines versus the stellar velocity dispersion for all the regions. Even though the scatter is large, it is possible to see that while most of the CNSFRs with stellar velocity dispersion below ∼40 km s^{-1} (all but two belonging to NGC 3310) show similar stellar, Hβ and [O III] velocity dispersions, the CNSFRs with stellar velocity dispersion above ∼40 km s^{-1} show a clear dichotomy with the [O III] profiles being systematically broader than those of Hβ. The Balmer emission lines are affected by the absorption produced by the underlying stellar population that depresses the lines (see a detailed discussion about this effect in H07, H09 and H10). To minimize the errors introduced by the underlying population, we defined a pseudo-continuum at the base of the line to fit the emission lines (for details, see Hägele et al. 2006). Nevertheless, the presence of a conspicuous underlying population could still be affecting the $\sigma_{\rm gas}$ derived from the Hβ emission lines. On the other hand, the fact that the regions with higher values of σ_* have systematically larger disagreement with the $\sigma_{\rm gas} = \sigma_*$ line could be related to that they are expected to be the most massive ones having the larger amount of stars and the most conspicuous underlying stellar populations.

As mentioned above, most of the observed CNSFR emission line profiles show wings detectable in both the Hβ hydrogen recombination line and the [O III] forbidden line. These wings can be attributed to the presence of a component broader than the core of the line. To investigate the origin of this broad component, we have assumed that it can be represented by a Gaussian profile. It should be kept in mind, however, that given that we do not have an a priori scenario for the origin of the broad component, there is no justification to assume a Gaussian profile either, apart from the fact that this assumption simplifies the analysis. If we assume that the wings are due to stellar winds, the broad component profile should be that of an expanding shell, i.e. a very flat top profile in which case the fluxes of the broad component obtained with a broad Gaussian will be overestimated and the dispersion of the narrow component will be underestimated. Yet, the best Gaussian fits involved two different components for the gas: a narrow component with velocity dispersions lower than the stellar one and a broad component with a velocity dispersion similar to or slightly larger than that measured for the stars. The resulting values of the multiple Gaussian fit to the observed profiles for both Hβ and [O III] narrow and broad components are listed in Tables 2 and 3.

In Figs 4 and 5, we show the velocity dispersion of the narrow and broad Gaussian components of Hβ and [O III], respectively, versus the stellar velocity dispersion. The narrow components of both Hβ and [O III] span a similar range in velocity dispersion with an average value of ∼23 km s^{-1}. On the other hand, the values of the velocity dispersion of the broad component of Hβ are similar to those of the stellar velocity dispersion, while the broad component of the [O III] line shows, in most cases, values of σ in excess of the stellar one. The correlation coefficient of the broad component of both Hβ and [O III] with the stellar velocity dispersion is much smaller than 0.5 indicating basically no correlation.

Bearing in mind that we may overinterpret the results of what is in reality a small sample, the fact that the narrow component of the gas in the CNSFRs in three different galaxies is, inside the error bars, roughly constant suggests that it may be originated in an inner

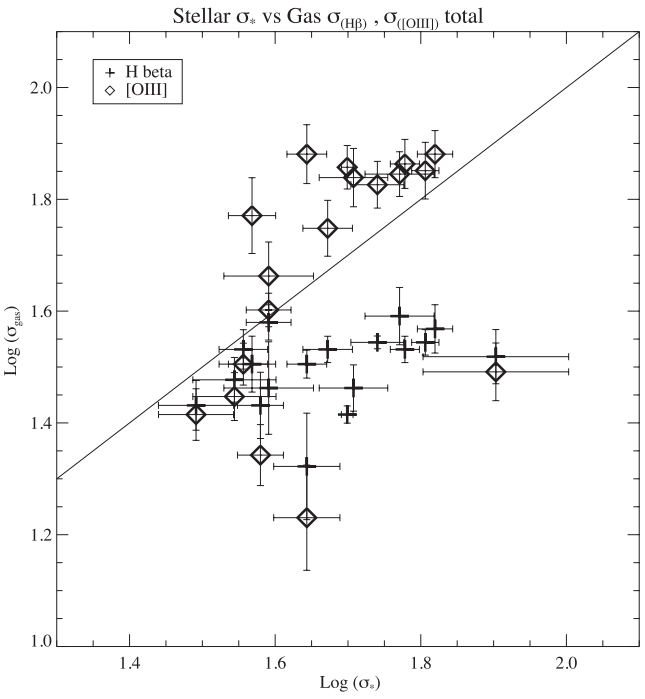

Figure 3. Gaseous versus stellar velocity dispersions from single-Gaussian fits. Pluses correspond to Hβ while open diamonds correspond to [O III]. The continuous line represents $\sigma_{\rm gas} = \sigma_{\rm stars}$.

[1] Image Reduction and Analysis Facility, distributed by NOAO, operated by AURA, Inc., under agreement with NSF.

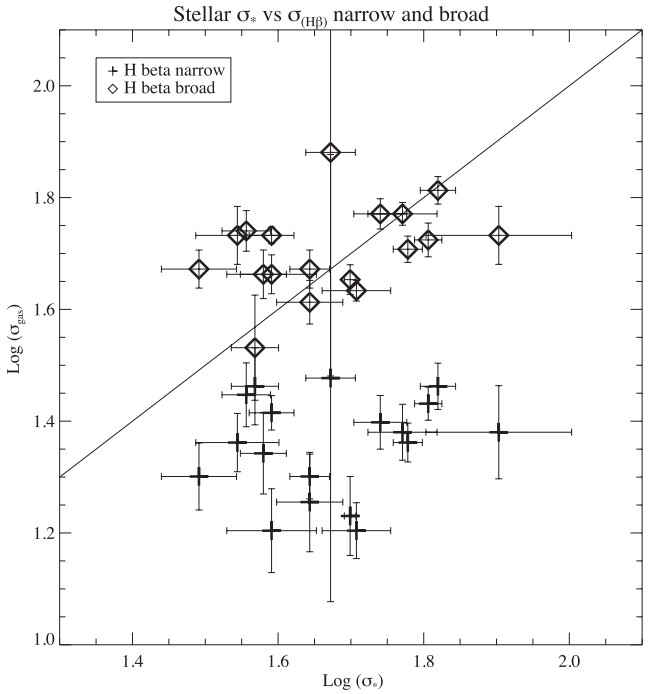

Figure 4. Gaseous (Hβ) versus stellar velocity dispersions for all the observed circumnuclear regions. The continuous line represents $\sigma_{\rm gas} = \sigma_{\rm stars}$.

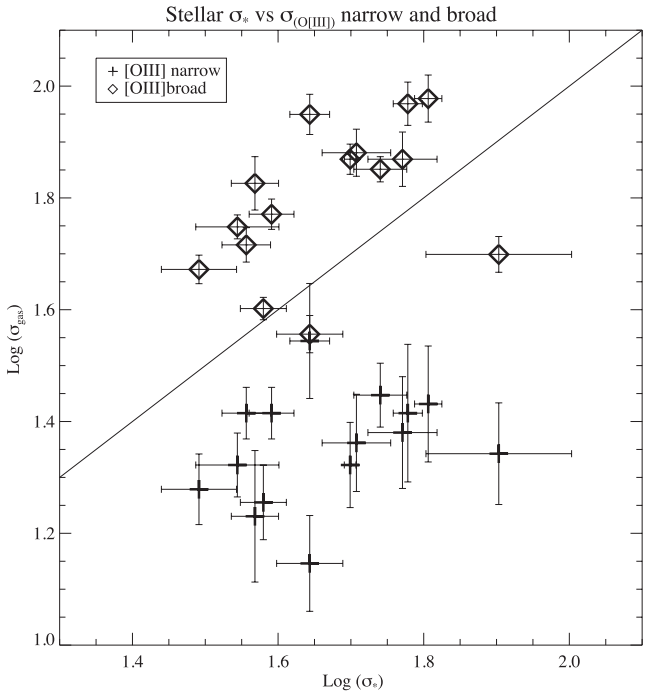

Figure 5. Gaseous (O[III]) versus stellar velocity dispersions for all the observed circumnuclear regions. The continuous line represents $\sigma_{\rm gas} = \sigma_{\rm stars}$.

disc that would be mainly supported by rotation. On the other hand, the stars and the gas responsible for the broad component could be related to the star-forming regions themselves and therefore would be mostly supported by dynamical pressure (see Pizzella et al. 2004, and references therein). This could, in principle, correspond to the gas response to the gravitational potential of the stellar cluster, thus explaining the coincidence with the stellar velocity dispersion in most cases for the broad component of the Hβ line. To disentangle the origin of the two different kinematical components, it will be necessary to map these regions with higher spectral and spatial resolution and much better signal-to-noise (S/N) ratio in particular for the [O III] lines.

The development of the integral field unit (IFU) instruments to perform 3D spectroscopy during the last few years has provided the spatial coverage required to study extended galactic or extragalactic star-forming regions (see e.g. García-Benito et al. 2010; Monreal-Ibero et al. 2010, 2011; Rosales-Ortega et al. 2010, 2011; López-Sánchez et al. 2011; Pérez-Montero et al. 2011; Sánchez et al. 2011, 2012b; Kehrig et al. 2012; Firpo et al. 2013; James et al. 2013b; López-Hernández et al. 2013). Recently, the first results of very powerful surveys of galaxies using IFU instruments have been released. The Calar Alto Legacy Integral Field Area survey is obtaining spatially resolved spectroscopic information of a selected sample of ∼600 galaxies in the Local Universe (Sánchez et al. 2012a). This survey has an effective spatial resolution of about 2 arcsec per fibre, and the final spectral resolution in full width at half-maximum is ∼6.5 Å (i.e. $\sigma \sim 150$ km s^{-1}) for the V500 grating and ∼2.7 Å (i.e. $\sigma \sim 85$ km s^{-1}) for the V1200. These instrumental configurations are not enough to disentangle the origin of the two different kinematical components with the required accuracy. The possibility of a future survey performed using the Sydney-AAO Multi-object Integral field spectrograph would be better for our purposes since its higher spectral resolution is $R = \lambda/\Delta\lambda \sim 13\,000$ (i.e. $\sigma \sim 23$ km s^{-1} at 4861 Å), and each fibre subtends 1.6 arcsec on the sky (Croom et al. 2012). However, medium- or high-dispersion slit spectroscopy is a better option for spectrophotometry, or when the object is very compact, or even extended but with a few star-forming knots. This is also the case when good spatial and spectral resolution and simultaneous wide spectral coverage are required (see e.g. Hägele et al. 2006, 2008, 2011, 2012; H07; H09; H10; Cumming et al. 2008; Hägele 2008; Firpo et al. 2010, 2011; López-Sánchez & Esteban 2009, 2010a,b; López-Sánchez 2010; Amorín et al. 2012).

3.2 Effects on abundance estimates

The presence of two kinematically segregated gaseous components could have an effect on the classification of the activity in the central regions of galaxies through diagnostic diagrams and also on abundance determinations if they are made from low-dispersion spectra by biasing the line ratios involved (see e.g. Esteban & Vilchez 1992; López-Sánchez et al. 2007; Hägele et al. 2012; James et al. 2013a,b). The only line ratio available from our data for the two kinematically separated components is [O III]/Hβ, whose logarithmic ratios are listed in Table 4. We find that in all the CNSFRs of NGC 2903 and NGC 3351 ([O III]/Hβ)$_{\rm narrow}$ < ([O III]/Hβ)$_{\rm broad}$, which indicates a higher excitation for the broad component gas. In the case of NGC 3351, the mean value of log ([O III]/Hβ)$_{\rm narrow}$ is −1.57 as compared to −0.93 for the same line ratio of the broad components, while a value of −1.04 is obtained from a single-Gaussian fit (see fig. 12 in H07). In these cases, the broad component contributes more than 80 per cent to the [O III] total flux while this contribution is smaller than 40 per cent for the Hβ line. This is not the case for the CNSFRs of NGC 3310 for which the contribution by the broad component to both the [O III] and Hβ emission line fluxes is similar and about 50 per cent which maintains the [O III]/Hβ ratio almost constant.

Fig. 6 shows a histogram of the logarithmic [O III]/Hβ ratio for the different components of the gas, broad and narrow, and also for the

Table 4. Logarithm of the [O III]5007/Hβ line ratio.

Region	log([O III]5007/Hβ)		
	One component	Narrow	Broad
	NGC 2903		
R1+R2	-1.03 ± 0.05	-1.64 ± 0.09	-0.76 ± 0.10
R1+R2	-0.92 ± 0.07	-1.51 ± 0.11	-0.57 ± 0.14
R4	-0.78 ± 0.11	-1.01 ± 0.10	-0.71 ± 0.15
R7	-0.78 ± 0.10	-1.79 ± 0.12	-0.40 ± 0.18
	NGC 3310		
R1+R2	0.42 ± 0.01	0.39 ± 0.01	0.45 ± 0.03
R4	0.28 ± 0.01	0.28 ± 0.01	0.28 ± 0.04
R4+R5	0.42 ± 0.01	0.39 ± 0.01	0.44 ± 0.03
R6	0.28 ± 0.01	0.30 ± 0.01	0.28 ± 0.06
S6	0.21 ± 0.01	0.21 ± 0.01	0.22 ± 0.08
R7	0.23 ± 0.01	0.21 ± 0.01	0.32 ± 0.09
R10	0.19 ± 0.01	0.20 ± 0.04	0.20 ± 0.08
	NGC 3351		
R2	-1.07 ± 0.06	-1.66 ± 0.08	-0.93 ± 0.12
R2	-1.01 ± 0.06	-1.55 ± 0.08	-0.96 ± 0.13
R3	-1.10 ± 0.06	-1.57 ± 0.07	-0.93 ± 0.10
R3	-1.00 ± 0.06	-1.52 ± 0.09	-0.89 ± 0.10

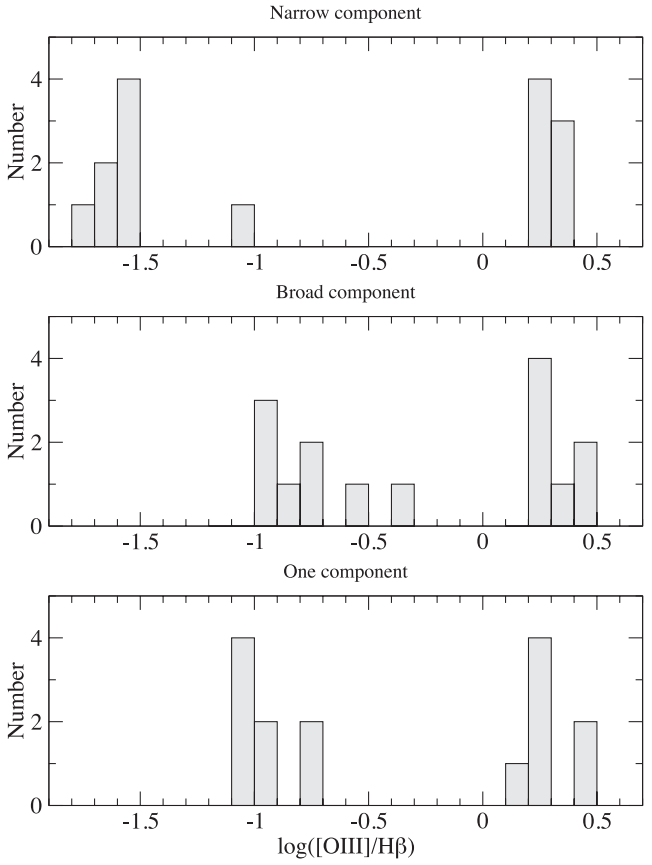

Figure 6. Histogram of the logarithmic [O III]/Hβ ratio for the different gaseous kinematic components compared to values derived from single-Gaussian fits.

case of a single-Gaussian fit (one component). It can be seen that for the CNSFRs of NGC 2903 and NGC 3351, the gas showing different velocity dispersions also shows different ionization properties with the broad component one showing a higher degree of excitation (see also Table 4). The data with the highest [O III]/Hβ ratio correspond to the regions in NGC 3310 for which no differences are found among the different cases.

3.3 σ–L and M–L relations

Fig. 7 shows the distribution of the CNSFRs in the L(Hα) versus σ plane. In the left column (upper panel), we plot the logarithm of the total Hα luminosity (values taken from the literature corrected for extinction) versus the gas velocity dispersion derived using a single-Gaussian fit. In the middle and lower panels, we show the same relation but for the Hα luminosity of the narrow [$L_{\rm n}$(Hα)] and broad [$L_{\rm b}$(Hα)] components of the two-Gaussian fits derived using the EMf estimated from the fit to the Hβ emission line, versus the corresponding velocity dispersion given by the multi-Gaussian fit ($\sigma_{\rm n}$ and $\sigma_{\rm b}$, respectively). The linear fits from Bosch, Terlevich & Terlevich (2002, hereafter B02) (dashed line) and Chávez et al. (2012, hereafter Ch12) (solid line) are also shown. These data correspond to 'young' single clusters in well-studied giant extragalactic H II regions. They comprise the structureless entities in the regions free of bubbles and shells which are supposed to appear at more evolved phases of evolution. These lines may be taken as the locus of virialized structures sampled by these compact emission knots.

Contrary to what is found for the compact emission line knots in nearby spirals by B02 and Ch12, no correlation is found between L(Hα) and σ either for single-Gaussian fits or for individual kinematical components; only three of our CNSFRs lie on top of the locus of virialized objects for the single-Gaussian fit case. A weak correlation seems to emerge for the narrow kinematical component of hydrogen that is maintained for the broad component although shifted to higher velocity dispersions. At any rate, the large dispersion of the data seems to be a common feature.

A certain degree of scatter in the diagram is expected related to the age evolution of the ionizing regions which would lower their Hα luminosity while keeping their velocity dispersion almost constant. The presence of this effect is reinforced by the fact that the three regions on top of the B02 and Ch12 lines are those with the largest EWs of Hβ (lower age) and therefore should be expected to be the less evolved ones.

A correction for this effect can be made by using the same expression employed for the estimation of the mass of the ionizing clusters, using a reference value for the EW of Hβ for an age lower than 3 Myr, i.e. EW(Hβ)$_0$ = 150 Å,

$$L(\mathrm{H}\alpha)_{\rm Corrected} = L(\mathrm{H}\alpha)_{\rm Observed} 10^{[44.48 + 0.86\ \log[\mathrm{EW}(\mathrm{H}\beta)_0]}. \quad (7)$$

The panels on the right column of Fig. 7 show the correlations just discussed once these evolutionary corrections have been applied. The net result is a considerable reduction of the scatter thus suggesting that the EW of Hβ (i.e. age) is the second parameter underlying the L(Hα) versus σ relation.

The stellar velocity dispersion behaves similarly to the broad component of the emission lines, albeit with larger dispersion.

It is of major interest to find out how widespread is the presence of two distinct components in the emission lines of these ionized regions. First, a change in position in the diagnostic diagrams would certainly affect the classification of the activity in the central regions of the concerned galaxies. Secondly, it will affect the inferences about the nature of the source of ionization in the two components. Thirdly, it could have an influence on the gas abundance determinations given that the ratio of the narrow to the broad components of Hβ is, in most cases, about 1/2.

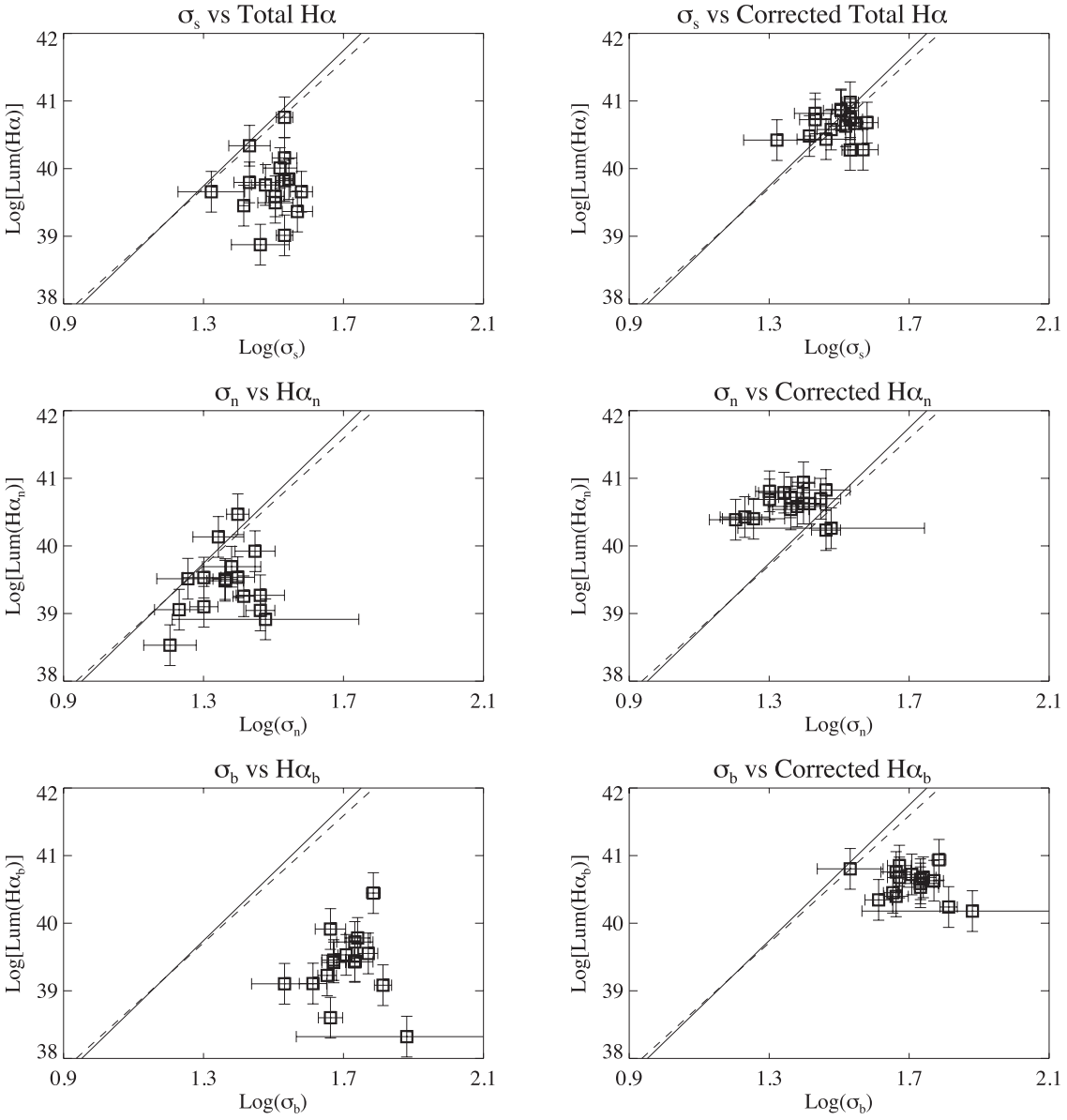

Figure 7. log(σ)− log(L) relations for the observed CNSFRs. Panels show the relations derived for the velocity dispersions of the gas using a single-Gaussian fit (top), narrow components (centre) and broad components (bottom), respectively. The panels on the right show the result after correcting the luminosity for evolution (see the text). The lines correspond to a linear fit to 'young' giant H II regions, plotted as a reference value; B02 (dashed line) and Chávez et al. 2012 (solid line).

Clearly, it is not possible to use global line ratios to estimate gaseous abundances if the permitted and forbidden line fluxes are originated in different kinematic systems.

We analyse the relation between the Hα luminosities of the broad component and the derived masses for the CNSFRs. Fig. 8 shows the relation between the logarithm of the upper limit to the dynamical masses and log(L(Hα)$_b$), together with the dynamical (M_{dyn}) and Keplerian (M_{Kep}) masses of Wolf–Rayet (WR) galaxies derived by López-Sánchez (2010, hereafter LS10). Values of M_{dyn} were estimated from H I radio observations considering the inclination-corrected maximum rotation velocity, which is obtained at the maximum radius observed in their deep optical images, and assuming virial equilibrium. As was pointed out by LS10, since the extension of the neutral gas is usually larger than the extension of the stellar component, their values of M_{dyn} may be underestimated, although they can be used as a rough estimation of the total mass of the galaxies. The M_{Kep} were estimated from the kinematics of the ionized gas. The Keplerian masses are lower than the dynamical ones, as expected, in almost all cases (see fig. 11 of LS10), with the more massive galaxies showing higher M_{Kep}/M_{dyn} ratios. This fact indicates that the kinematics derived from the ionized gas is not completely appropriate for deriving the total dynamical mass in this kind of objects (LS10).

The upper limits to the dynamical masses of the CNSF complexes seem to follow a sequence when we compare them with those masses derived for the WR galaxies (see Fig. 8). Our objects are located in the lower part of the sequence, showing lower masses and lower Hα luminosities. A fitting to the logarithmic dynamical mass–luminosity (M–L) relation shown by the CNSFRs (solid line in the figure) gives the following expression:

$$\log(L(\mathrm{H}\alpha)_b) = (0.8 \pm 0.1)\log(M_*) + (33 \pm 1). \quad (8)$$

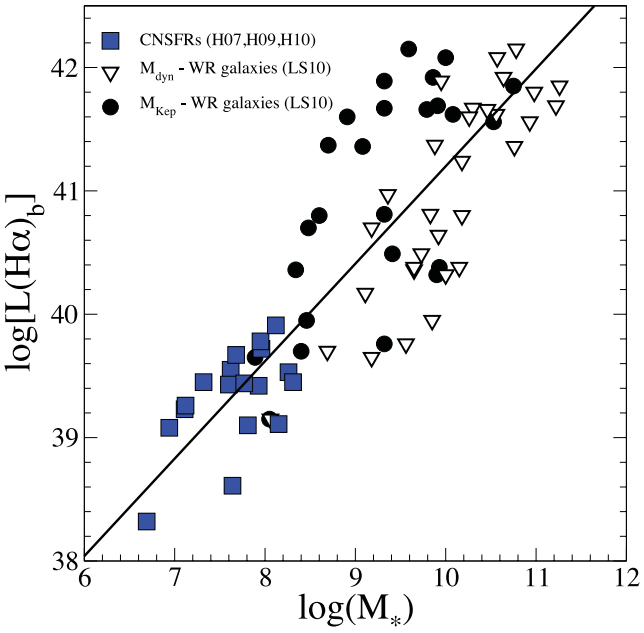

Figure 8. Hα luminosity versus cluster dynamical mass for the observed CNSFRs (squares). Similar data on WR galaxies from the sample of LS10 are shown for comparison. In the latter case, both dynamical (inverted triangles) and Keplerian (circles) masses are plotted.

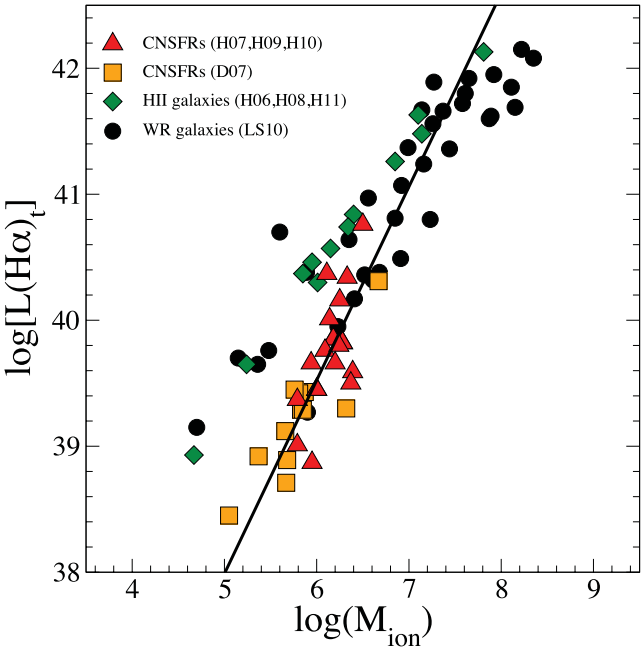

Figure 9. Hα luminosity versus ionizing star cluster mass for the observed CNSFRs (triangles and squares). Similar data on WR galaxies (solid circles) and H II galaxies (diamonds) are also shown.

The relation between the masses of the ionizing clusters of the CNSFRs and their Hα luminosities is shown in Fig. 9. In spite of depending on a theoretical relationship which is only function of the Hα luminosity and the EW of the Hβ emission line, the CNSFRs (including the objects studied by D07) seem to define a different sequence from the one followed by the H II galaxies studied in Hägele et al. (2006, 2008, 2011, hereafter H06, H08 and H11), and the WR galaxies analysed by LS10 (see López-Sánchez & Esteban

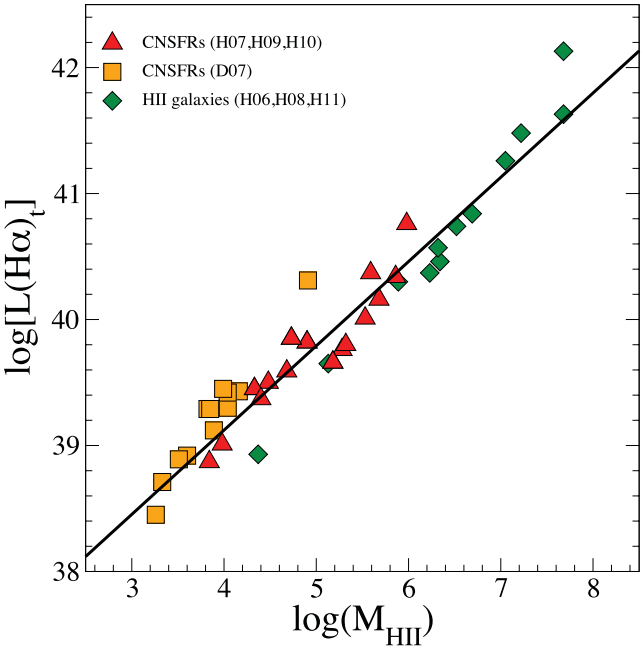

Figure 10. Hα luminosity versus ionized hydrogen mass for the observed CNSFRs (squares and triangles). Similar data on H II galaxies (diamonds) are also shown.

2008 for a detailed description of the optical data). This could be due to underestimating the EW(Hβ) hence overestimating the masses of the ionizing star clusters. The dilution of the EW(Hβ) can be caused by the presence of an old underlying stellar population with wider Hβ absorption that rises the continuum and depresses the emission line (see a detailed discussion about this effect in D07). In addition, the low EW(Hβ) values for CNSFRs might come from the contribution to the observed continuum by the galactic bulge population. Dors et al. (2008) suggest that the combination of an underlying older population from the region itself and stars from the bulge could account for the observed effect. The strong influence that the measured EW has on the derived mass of the ionizing cluster indicates that the trend observed in Figs 8–10 can be attributed to the fact that the contamination by the bulge will be relatively stronger as the intrinsic luminosity of the starburst diminishes.

This effect is more evident for the less massive objects. The most massive CNSFRs tend to be located around the position occupied by the H II and WR galaxies of similar cluster ionizing masses. The effect of the presence of an underlying old stellar population over the EW of Hβ in this kind of emission line galaxies with recent episodes of star formations is relatively small since the continuum of the bright young stellar population dominates the light in this spectral range [see a detailed discussion about the contributions of the different stellar populations to the EW(Hβ) in Pérez-Montero et al. (2010) and H11].

The solid line in Fig. 9 represents the fit to the logarithmic relation between $M_{\rm ion}$ and total Hα luminosities for the CNSFRs, and is given by

$$\log(L(\mathrm{H}\alpha)_{\rm t}) = (1.5 \pm 0.4)\,\log(M_{\rm ion}) + (30 \pm 2). \quad (9)$$

Finally, in Fig. 10 we have plotted the relation between the masses of the ionized gas and the total Hα luminosities, together with the CNSFRs presented in D07 and the H II galaxies studied in H06, H08 and H11. The fitting to this relation for the CNSFRs gives

$$\log(L(\mathrm{H}\alpha)_{\rm t}) = (0.67 \pm 0.07)\,\log(M_{\rm H\,II}) + (36.4 \pm 0.3). \quad (10)$$

4 SUMMARY AND CONCLUSIONS

We have analysed the results derived by H07, H09 and H10 using high-spectral-resolution data of 17 CNSFRs belonging to 3 barred spiral galaxies: NGC 2903, NGC 3310 and NGC 3351. The stellar velocity dispersions were measured from the CaT lines at λλ8494, 8542, 8662 Å. The gas velocity dispersions have been measured by Gaussian fits to the Hβ λ4861 Å and the [O III] λ5007Å emission lines.

Stellar velocity dispersions range between 31 and 80 km s^{-1}. In the case of NGC 2903 and NGC 3351 (σ_* between 37 and 64, and between 39 and 66 km s^{-1}, respectively), these values are about 25 km s^{-1} larger than those measured for the gas from the Hβ emission line using a single-Gaussian fit. For NGC 3310, the stellar (between 31 and 80 km s^{-1}) and gas (Hβ) velocity dispersions are in relatively good agreement, the stellar ones being marginally larger.

Single-Gaussian fitting to the [O III] 5007 Å line provides gas velocity dispersions for NGC 2903 and NGC 3351 that are very similar to – or marginally larger than – the stellar ones. The gas velocity dispersion derived from a single-Gaussian fit for the [O III] line in NGC 3310 is also comparable to the stellar velocity dispersion but, contrary to what was found in the other two galaxies, its value is also very similar to that derived using Hβ.

The best Gaussian fits for Hβ, however, involved two different components for the gas: a 'broad component' with a velocity dispersion similar to that measured for the stars for NGC 2903 and NGC 3351, and about 20 km s^{-1} larger than the stellar one for NGC 3310, and a 'narrow component' with a velocity dispersion lower than the stellar one by about 30 km s^{-1}. This narrow component shows a relatively constant value for the two emission lines (Hβ and [O III]), close to 23 km s^{-1} (with scatter errors of 1.1 and 1.4 km s^{-1}, respectively) for all the studied CNSFRs.

The [O III]/Hβ ratio distribution shows that the two systems are clearly segregated for the high-metallicity regions of NGC 2903 and NGC 3351, with the narrow component having the lowest excitation. In the regions of the low-metallicity galaxy, NGC 3310, these two components and those values derived using the single-Gaussian fit are very similar.

Values for the upper limits to the dynamical masses estimated from the stellar velocity dispersion using the virial theorem for the studied CNSF complexes are in the range between 4.9×10^6 and 1.9×10^8 M$_\odot$. Masses of the ionizing stellar clusters of the CNSFRs have been derived from their Hα luminosities and the EW of the Hβ emission line under the assumption that the regions are ionization bound and have a single stellar population, and without taking into account any photon absorption by dust. These masses of the regions studied in the three galaxies vary between 8.0×10^5 and 4.9×10^6 M$_\odot$. Therefore, the ratio of the ionizing stellar population to the total dynamical mass, under these hypotheses, is between 0.01 and 0.16. The derived masses for the ionized gas, also from their Hα luminosities, vary between 7.0×10^3 and 7.2×10^5 M$_\odot$.

The distribution of the CNSFRs in the $\log(\sigma) - \log(L)$ plane presents a correlation between their luminosities and velocity dispersions, albeit with large dispersion. The single-Gaussian fit for our CNSFRs is slightly shifted to lower luminosities and/or higher values of the gas velocity dispersion with respect to the regression found for virialized systems, although the general behaviour is similar to what was found by Firpo et al. (2010, 2011) for giant extragalactic H II regions of NGC 6070 and NGC 7479, and star-forming regions belonging to the Haro 15 galaxy, respectively. The narrow components of the multi-Gaussian fits to the emission lines of the CNSFRs lie very close to this linear regression, with the brightest objects around the regression, while the broad components are located in a parallel sequence shifted towards lower luminosities and/or higher velocity dispersions. We have been able to considerably reduce the observed scatter in the L–σ relation applying an evolutionary correction that depends on the age of the regions through their EWs of Hβ. The EW(Hβ) seems to be a second-order parameter underlying this relation. Although the stellar velocity dispersions have a large scatter, they present a similar behaviour to the broad component ones.

We have also analysed the relations between the total Hα luminosities and the derived masses for the studied CNSFRs. The upper limits to the dynamical masses of the CNSF complexes seem to be located in the lower part of a sequence showing lower masses and lower Hα luminosities than those masses derived for WR galaxies by LS10. The distribution of the masses of the ionizing clusters of the CNSFRs, including the regions presented by D07, falls outside a sequence defined by the H II and WR galaxies analysed by H06, H08 and H11, and by LS10, respectively. The CNSFRs are also arranged in a steeper slope sequence which is located towards lower values of the Hα luminosities or higher masses, except for the most massive regions. This occurs although the ionizing stellar masses depend on a theoretical relationship which is a function only of the Hα luminosity and the EW of the Hβ emission line. Underestimating EW(Hβ) would produce an overestimation of these masses. We have to remark that, according to our findings, the super star clusters in CNSFRs seem to contain composite stellar populations (see e.g. H07 and D07). The contribution of stars from the bulge projected along the line of sight (Dors et al. 2008) has also to be considered. Although the youngest population of star-forming complexes dominates the UV light and is responsible for the gas ionization, it represents only about 10 per cent of the total mass belonging to the region. This can explain the low EWs of the emission lines generally measured in these regions. This may well apply to the case of other super star clusters, and therefore conclusions drawn from fits of single stellar population models should be taken with caution (e.g. McCrady, Gilbert & Graham 2003; Larsen, Brodie & Hunter 2004). On the other hand, the relation between the derived masses of the ionized gas of the CNSFRs and the Hα luminosities follows the same sequence defined by the H II galaxies presented by H06, H08 and H11.

A possible scenario for understanding the behaviour of CNSFRs in the L–σ and $\sigma_{\rm gas}$–σ_* diagrams is to assume that the narrow component of hydrogen belongs to an inner rotating disc; therefore, its velocity dispersion is approximately constant for all the CNSFRs. On the other hand, the broad component of hydrogen would be related to the CNSF complexes themselves, and therefore its velocity dispersion would be expected to be similar to the stellar one. [The velocity dispersion of collisionally excited [O III] is in some cases larger than this, a behaviour also seen in Seyfert 2 galaxies, but not in Seyfert 1 (see Jiménez-Benito et al. 2000).] In that case, all the Hα derived quantities for the CNSFRs should use the luminosity of the broad component which is about one half of the total. The fact that there is a distinctive behaviour in the L(Hα) versus $M_{\rm ion}$ in disc H II regions and CNSFRs in the sense of showing a larger mass for a given Hα luminosity could be related to the H II regions being matter bounded, that is photons are escaping the region. Incidentally (or not so) these photons would ionize the hydrogen in the inner disc and therefore would in part be responsible for the narrow component of hydrogen. All this would be consistent with the picture of some CNSFRs undergoing 'residual' star formation that involves about 10 per cent of the total dynamical mass. This behaviour would be related to the evolution of the region with the

ones showing the larger EW(Hβ), that is the younger ones, having more hydrogen available and thus being less prone to photon escape. The SFRs for the CNSFRs should also be derived from the luminosity of the broad component of Hα and would be about half the ones derived from the total Hα fluxes. This would explain the lack of detection at radio wavelengths (Hägele et al. 2010b).

The existence of more than one velocity component in the ionized gas corresponding to kinematically distinct systems deserves further study. Several results derived from the observations of the different emission lines could be affected, among others: the classification of the activity in the central regions of galaxies, the inferences about the nature of the source of ionization, the gas abundance determinations, the number of ionizing photons from a given region and any quantity derived from them, as well as the σ–L and M–L relations. To disentangle the origin of these two components and to discriminate among the different stellar population contributions to the continuum of the regions, it will be necessary to map these regions with high spectral and spatial resolution and much better S/N ratio. High-resolution 2D spectroscopy with IFUs would be the ideal tool to approach this issue.

ACKNOWLEDGEMENTS

We are grateful to the referee, Ángel López-Sánchez, for a thorough reading of the manuscript and for his constructive comments and suggestions.

The WHT is operated on the island of La Palma by the Isaac Newton Group in the Spanish Observatorio del Roque de los Muchachos of the Instituto de Astrofísica de Canarias. We thank the Spanish allocation committee (CAT) for awarding observing time.

Some of the data presented in this paper were obtained from the Multimission Archive at the Space Telescope Science Institute (MAST). STScI is operated by the Association of Universities for Research in Astronomy, Inc., under NASA contract NAS5-26555. Support for MAST for non-*HST* data is provided by the NASA Office of Space Science via grant NAG5-7584 and by other grants and contracts.

This research has made use of the NASA/IPAC Extragalactic Database (NED) which is operated by the Jet Propulsion Laboratory, California Institute of Technology, under contract with the National Aeronautics and Space Administration and of the SIMBAD data base, operated at CDS, Strasbourg, France.

Financial support for this work has been provided by the Spanish Ministerio de Educación y Ciencia (AYA2007-67965-C03-03 and AYA2010-21887-C04-03). Partial support from the Comunidad de Madrid under grant S2009/ESP-1496 (ASTROMADRID) is acknowledged. ET and RT are grateful to the Mexican Research Council (CONACYT) for support under grants CB2005-01-49847F and CB2008-01-103365.

REFERENCES

Amorín R., Vílchez J. M., Hägele G. F., Firpo V., Pérez-Montero E., Papaderos P., 2012, ApJ, 754, L22
Boily C. M., Lançon A., Deiters S., Heggie D. C., 2005, ApJ, 620, L27
Bosch G., Terlevich E., Terlevich R., 2002, MNRAS, 329, 481 (B02)
Bottinelli L., Gouguenheim L., Paturel G., de Vaucouleurs G., 1984, A&AS, 56, 381
Cerviño M., Valls-Gabaud D., Luridiana V., Mas-Hesse J. M., 2002, A&A, 381, 51
Chávez R., Terlevich E., Terlevich R., Plionis M., Bresolin F., Basilakos S., Melnick J., 2012, MNRAS, 425, L56 (Ch12)
Colina L., González-Delgado R., Mas-Hesse J. M., Leitherer C., 2002, ApJ, 579, 545
Croom S. M. et al., 2012, MNRAS, 421, 872
Cumming R. J., Fathi K., Östlin G., Marquart T., Márquez I., Masegosa J., Bergvall N., Amram P., 2008, A&A, 479, 725
de Vaucouleurs G., de Vaucouleurs A., Corwin H. G., Jr, Buta R. J., Paturel G., Fouque P., 1991, Third Reference Catalogue of Bright Galaxies. Vol. 1–3, XII, Springer-Verlag, New York, p. 2069
Díaz A. I., Álvarez-Álvarez M., Terlevich E., Terlevich R., Portal M. S., Aretxaga I., 2000a, MNRAS, 311, 120
Díaz A. I., Castellanos M., Terlevich E., Luisa García-Vargas M., 2000b, MNRAS, 318, 462
Díaz A. I., Terlevich E., Castellanos M., Hägele G. F., 2007, MNRAS, 382, 251 (D07)
Dors O. L., Jr, Storchi-Bergmann T., Riffel R. A., Schimdt A. A., 2008, A&A, 482, 59
Esteban C., Vilchez J. M., 1992, ApJ, 390, 536
Firpo V., Bosch G., Hägele G. F., Morrell N., 2010, MNRAS, 406, 1094
Firpo V., Bosch G., Hägele G. F., Díaz A. I., Morrell N., 2011, MNRAS, 414, 3288
Firpo V., Bosch G., Hägele G. F., Díaz R., 2013, ApJ, submitted
Fleck J.-J., Boily C. M., Lançon A., Deiters S., 2006, MNRAS, 369, 1392
García-Benito R. et al., 2010, MNRAS, 408, 2234
García-Vargas M. L., Bressan A., Díaz A. I., 1995, A&AS, 112, 35
González-Delgado R. M., Heckman T., Leitherer C., Meurer G., Krolik J., Wilson A. S., Kinney A., Koratkar A., 1998, ApJ, 505, 174
Graham J. A. et al., 1997, ApJ, 477, 535
Hägele G. F., 2008, PhD thesis, Universidad Autónoma de Madrid
Hägele G. F., Pérez-Montero E., Díaz A. I., Terlevich E., Terlevich R., 2006, MNRAS, 372, 293 (H06)
Hägele G. F., Díaz A. I., Cardaci M. V., Terlevich E., Terlevich R., 2007, MNRAS, 378, 163 (H07)
Hägele G. F., Díaz A. I., Terlevich E., Terlevich R., Pérez-Montero E., Cardaci M. V., 2008, MNRAS, 383, 209 (H08)
Hägele G. F., Díaz A. I., Cardaci M. V., Terlevich E., Terlevich R., 2009, MNRAS, 396, 2295 (H09)
Hägele G. F., Díaz A. I., Cardaci M. V., Terlevich E., Terlevich R., 2010a, MNRAS, 402, 1005 (H10)
Hägele G. F. et al., 2010b, MNRAS, 406, 1675
Hägele G. F., García-Benito R., Pérez-Montero E., Díaz A. I., Cardaci M. V., Firpo V., Terlevich E., Terlevich R., 2011, MNRAS, 414, 272 (H11)
Hägele G. F., Firpo V., Bosch G., Díaz A. I., Morrell N., 2012, MNRAS, 422, 3475
Harper D. A., Jr, Low F. J., 1973, ApJ, 182, L89
Ho L. C., Filippenko A. V., 1996a, ApJ, 466, L83
Ho L. C., Filippenko A. V., 1996b, ApJ, 472, 600
James B. L., Tsamis Y. G., Barlow M. J., Walsh J. R., Westmoquette M. S., 2013a, MNRAS, 428, 86
James B. L., Tsamis Y. G., Walsh J. R., Barlow M. J., Westmoquette M. S., 2013b, MNRAS, 430, 2097
Jiménez-Benito L., Díaz A. I., Terlevich R., Terlevich E., 2000, MNRAS, 317, 907
Kehrig C. et al., 2012, A&A, 540, A11
Kennicutt R. C., Jr, 1998, ARA&A, 36, 189
Kennicutt R. C., Jr, Keel W. C., Blaha C. A., 1989, AJ, 97, 1022
Larsen S. S., Brodie J. P., Hunter D. A., 2004, AJ, 128, 2295
Leitherer C., Heckman T. M., 1995, ApJS, 96, 9
López-Hernández J., Terlevich E., Terlevich R., Rosa-González D., Díaz Á., García-Benito R., Vílchez J., Hägele G., 2013, MNRAS, 430, 472
López-Sánchez A. R., 2010, A&A, 521, A63 (LS10)
López-Sánchez A. R., Esteban C., 2008, A&A, 491, 131
López-Sánchez A. R., Esteban C., 2009, A&A, 508, 615
López-Sánchez A. R., Esteban C., 2010a, A&A, 516, A104
López-Sánchez A. R., Esteban C., 2010b, A&A, 517, A85
López-Sánchez Á. R., Esteban C., García-Rojas J., Peimbert M., Rodríguez M., 2007, ApJ, 656, 168

López-Sánchez A. R., Mesa-Delgado A., López-Martín L., Esteban C., 2011, MNRAS, 411, 2076
Macchetto F., Colina L., Golombek D., Perryman M. A. C., di Serego Alighieri S., 1990, ApJ, 356, 389
McCrady N., Gilbert A. M., Graham J. R., 2003, ApJ, 596, 240
Miller J. S., Mathews W. G., 1972, ApJ, 172, 593
Monreal-Ibero A., Vílchez J. M., Walsh J. R., Muñoz-Tuñón C., 2010, A&A, 517, A27
Monreal-Ibero A., Relaño M., Kehrig C., Pérez-Montero E., Vílchez J. M., Kelz A., Roth M. M., Streicher O., 2011, MNRAS, 413, 2242
Morgan W. W., 1958, PASP, 70, 364
Pastoriza M. G., Dottori H. A., Terlevich E., Terlevich R., Diaz A. I., 1993, MNRAS, 260, 177
Pérez-Montero E., García-Benito R., Hägele G. F., Díaz Á. I., 2010, MNRAS, 404, 2037
Pérez-Montero E. et al., 2011, A&A, 532, A141
Pérez-Olea D., 1996, PhD thesis, Universidad Autónoma de Madrid
Pizzella A., Corsini E. M., Vega Beltrán J. C., Bertola F., 2004, A&A, 424, 447
Planesas P., Colina L., Pérez-Olea D., 1997, A&A, 325, 81
Relaño M., Beckman J. E., 2005, A&A, 430, 911
Rieke G. H., Lebofsky M. J., 1978, ApJ, 220, L37
Rieke G. H., Low F. J., 1972, ApJ, 176, L95
Rosales-Ortega F. F., Kennicutt R. C., Sánchez S. F., Díaz A. I., Pasquali A., Johnson B. D., Hao C. N., 2010, MNRAS, 405, 735
Rosales-Ortega F. F., Díaz A. I., Kennicutt R. C., Sánchez S. F., 2011, MNRAS, 415, 2439
Salpeter E. E., 1955, ApJ, 121, 161
Sánchez S. F., Rosales-Ortega F. F., Kennicutt R. C., Johnson B. D., Diaz A. I., Pasquali A., Hao C. N., 2011, MNRAS, 410, 313
Sánchez S. F. et al., 2012a, A&A, 538, A8
Sánchez S. F. et al., 2012b, A&A, 546, A2
Sérsic J. L., Pastoriza M., 1965, PASP, 77, 287
Sérsic J. L., Pastoriza M., 1967, PASP, 79, 152
Telesco C. M., Harper D. A., 1980, ApJ, 235, 392

This paper has been typeset from a TEX/LATEX file prepared by the author.